CHALMERS
UNIVERSITY OF TECHNOLOGY

Wideband mmWave Massive MIMO Channel Estimation and Localization

Downloaded from: https://research.chalmers.se, 2025-12-08 23:28 UTC

Citation for the original published paper (version of record):
Weng, S., Jiang, F., Wymeersch, H. (2023). Wideband mmWave Massive MIMO Channel Estimation and Localization. IEEE Wireless Communications Letters, 12(8): 1314-1318.
http://dx.doi.org/10.1109/LWC.2023.3270160

N.B. When citing this work, cite the original published paper.

© 2023 IEEE. Personal use of this material is permitted. Permission from IEEE must be obtained for all other uses, in any current or future media, including reprinting/republishing this material for advertising or promotional purposes, or reuse of any copyrighted component of this work in other works.

(article starts on next page)

Wideband mmWave Massive MIMO Channel Estimation and Localization

Shudi Weng, *Student Member, IEEE*, Fan Jiang, *Member, IEEE*, and Henk Wymeersch *Senior Member, IEEE*

***Abstract*—Spatial wideband effects are known to affect channel estimation and localization performance in millimeter wave (mmWave) massive multiple-input multiple-output (MIMO) systems. Based on perturbation analysis, we show that the spatial wideband effect is in fact more pronounced than previously thought and could significantly degrade performance if not properly considered in the algorithm design, even at moderate bandwidths. We propose a novel channel estimation method based on multidimensional ESPRIT algorithms per subcarrier, combined with unsupervised learning for pairing across subcarriers, which shows significant performance gain over existing schemes under wideband conditions.**

***Index Terms*—Wideband effect, ESPRIT, wideband localization, mmWave MIMO.**

I. Introduction

Integrated communication and localization has attracted increasing attention in 5G and beyond [1]–[3]. For one thing, massive multiple-input multiple-output (MIMO) and millimeter wave (mmWave) techniques have been demonstrated to significantly improve communication performance in terms of reliability, throughput, and scalability. For another, the deployment of large antenna arrays and the availability of large bandwidth at mmWave improve the angle and delay resolution, thus leading to high accuracy localization [4], [5].

The bridge between communication and localization is the propagation channel [3], [5], [6], since the communication quality is a function of the user equipment (UE) location via the channel's geometric parameters (including the angle-of-arrival (AOA), angle-of-departure (AOD), and time-of-arrival (TOA)), which are used both for communication and localization purposes [5]–[7]. Therefore, one of the main challenges in integrated localization and communication is to estimate the channel parameters, from which one can localize the UE and/or optimize the communication rate [5]–[9]. Channel estimation in massive MIMO mmWave communication systems can be divided into two categories. *On-grid methods* rely on a pre-defined dictionary to estimate the multipath components [10], [11], and thus are inherently limited by the dictionary size. In contrast, *off-grid methods* transform the channel estimation problem into an optimization problem [12]–[15] or provide direct solutions based on the problem structure [8], [16]–[18]. Among this last class of methods, an algorithm based on improved multidimensional folding (IMDF) and estimation of signal parameters via rotational invariant techniques (ESPRIT) has been applied in mmWave massive MIMO channel estimation [5]–[8], [13].

Most existing studies on ESPRIT for mmWave massive MIMO channel estimation assume a narrowband[1] channel model, which indicates that the bandwidth is relatively small and the array size is small [5]–[8]. As pointed out in [14], [15], when the array size and the system bandwidth become large, the spatial wideband effects (also known as the *beam-squint*) are non-negligible. In particular, spatial wideband introduces an undesired coupling of the angular frequencies in the frequency domain (corresponding to the delays) and the spatial domain (corresponding to the angles). To the best of our knowledge, channel parameter estimation under the spatial wideband effect was considered in a limited number of studies, e.g., [14], [15], [19]. The authors in [14], [15] explore the optimization methods to find the angle and delay iteratively, which requires good initial estimates and high complexity due to the iterative search. In [19], IMDF per subcarrier was proposed in order to reconstruct the channel, requiring multiple snapshot measurements over several coherence intervals to have the channel experience independent fading, which causes delays and leads to an ambiguous estimate of the channel parameters if the UE is moving. Besides, the pairing of parameters among subcarriers and performance evaluation in terms of spatial frequencies was not considered.

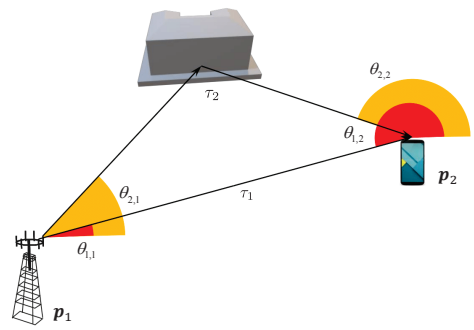

Fig. 1: Considered localization scenario with multipath. The objective of the UE is to estimate its location and clock bias based on the estimated AOA, AOD, and TOA of each path.

In this paper, we investigate a low-complexity ESPRIT[2] method for dealing with the wideband effect for wideband mmWave massive MIMO system with explicit pairing across subcarriers. The proposed method can operate with a single snapshot measurement and is evaluated in terms of both channel parameter estimation and positioning. Our contributions are summarized as follows: (i) we propose a novel combina-

[1]The term 'narrowband' refers to the array steering vectors being frequency-flat, while the overall channel response may be frequency-selective.

[2]The MD-ESPRIT-based approach from [18] is used, as (i) it has been shown to outperform the IMDF-based approach used in [19] in terms of angular frequency estimations, and (ii) it has lower computational complexity than tensor-based ESPRIT [20].

tion of ESPRIT-based channel estimation and clustering, for dealing with the wideband effect for mmWave massive MIMO channel estimation under spatial wideband propagations based on one snapshot observation; (ii) as part of this method, we introduce a novel pairing strategy to deal with the auto-pairing problem of path parameters, which will occur when the algorithm applies the singular value decomposition (SVD) on each subcarrier independently; (iii) we provide a tighter narrowband condition for localization, and have verified the proposed condition in simulations; (iv) we assess the performance of the proposed method against standard approaches and show that the proposed method has better performance, both in spatial frequency estimation and localization, even with relatively moderate spatial wideband effects.

Notations: The operations $\otimes$ and $\odot$ denote the Kronecker and Khatri-Rao (column-wise) products, respectively. The outer product is denoted by $\circ$, and the Hadamard product (element-wise) is denoted by $\bullet$. $\mathrm{vec_r}$ denotes vectorization by row. $\Im(\cdot)$ and $\Re(\cdot)$ denotes the imaginary and the real part, respectively.

II. System Model

Consider a massive MIMO orthogonal frequency division multiplexing (OFDM) system, which consists of a base station (BS) at location $\boldsymbol{p}_1 = (p_{x,1}, p_{y,1})$ equipped with a uniform linear array (ULA) of M_1-antenna elements and a UE at location $\boldsymbol{p}_2 = (p_{x,2}, p_{y,2})$ equipped with M_2-antenna ULA. There exist L resolvable propagation paths between the BS and UE. The system bandwidth is B, and the number of subcarriers is K, i.e., the subcarrier spacing is $\Delta f = B/K$. The frequency domain channel $\boldsymbol{\mathcal{H}} \in \mathbb{C}^{M_1 \times M_2 \times K}$, accounting for the spatial wideband effect [14], [15], collects all the channel elements $h_{m_1,m_2,k}$ from the m_1-th BS antenna to the m_2-th UE antenna over the k-th subcarrier as

$$h_{m_1,m_2,k} = \sum_{l=1}^{L} \breve{\alpha}_l e^{-j2\pi m_1 \phi_{l,k,1}} e^{-j2\pi m_2 \phi_{l,k,2}} e^{-j2\pi k \Delta f \tau_l}, \tag{1}$$

where $m_i \in \{0, \ldots, M_i - 1\}$ for $i \in \{1, 2\}$ and $k \in \{0, \ldots, K-1\}$, and

$$\phi_{l,k,i} = \phi_{l,i}\big(1 + \frac{k\Delta f}{f_\mathrm{c}}\big). \tag{2}$$

Here, $\breve{\alpha}_l = \alpha_l \exp(-j2\pi f_\mathrm{c} \tau_l)$, where α_l denotes the complex gain of the l-th path, including phase offsets, τ_l is the delay (TOA) of the l-th path. The normalized AOD and AOA are given by $\phi_{l,i} = d_i \sin\theta_{l,i}/\lambda_\mathrm{c}$, $i = 1, 2$, respectively, in which $\theta_{l,i}$ denotes the corresponding physical AOD and AOA of l-th path and d_i denotes the antenna spacing at BS and UE. Finally, f_c denotes the carrier frequency, and λ_c is the corresponding wavelength. For the line-of-sight (LOS) path ($l = 1$), $\tau_1 = \|\boldsymbol{p}_1 - \boldsymbol{p}_2\|/c + \Delta\tau$, $\theta_{1,1} = \arctan((p_{y,2} - p_{y,1})/(p_{x,2} - p_{x,1}))$, $\theta_{1,2} = \arctan((p_{y,1} - p_{y,2})/(p_{x,2} - p_{x,1}))$, where $\Delta\tau$ is the unknown clock bias. For the non-line-of-sight (NLOS) paths ($l \neq 1$), suppose that the incidence point of the l-th path is located at $\boldsymbol{p}'_l = (p'_{x,l}, p'_{y,l})$, then we have $\tau_l = (\|\boldsymbol{p}_1 - \boldsymbol{p}'_l\| + \|\boldsymbol{p}_2 - \boldsymbol{p}'_l\|)/c + \Delta\tau$, $\theta_{l,1} = \arctan[(p'_{y,l} - p_{y,1})/(p'_{x,l} - p_{x,1})]$, $\theta_{l,2} = \arctan[(p_{y,1} - p'_{y,l})/(p_{x,2} - p'_{x,l})]$.

The channel estimation is performed on pilot symbols (training sequences). Similar to [21], we perform the maximum likelihood channel estimation, and the resultant channel estimate over the k-th subcarrier is given by

$$\hat{\boldsymbol{H}}_k = \boldsymbol{H}_k + \boldsymbol{E}_k, \tag{3}$$

where $\boldsymbol{H}_k$ is the k-th slice of tensor $\boldsymbol{\mathcal{H}}$, and $\boldsymbol{E}_k$ denotes the channel estimation error, in which each entry is modeled as independent and identically distributed zero-mean Gaussian random variable. Finally, L is assumed to be known.[3]

III. Parallel ESPRIT-based Algorithm for Channel Parameter Estimation and Localization

From (1), we note that the channel parameters, i.e., AOAs, AODs, and delays, are related to angular frequencies. Hence, the estimation of the channel parameters from noisy $\hat{\boldsymbol{H}}_k$ can be transformed into a multi-dimensional (MD) harmonic retrieval (MHR) problem. In this section, we formulate the channel tensor of both wideband and narrowband models, analyze the narrowband condition, develop a parallel ESPRIT-based algorithm for channel parameter estimation and a pairing method across subcarriers. Based on the paired parameters, fusion across subcarriers is performed, and finally, the UE is localized.

A. Tensor Formulation of the Wideband Channel

The channel model from (1) can be formulated with a tensor $\boldsymbol{\mathcal{H}} \in \mathbb{C}^{M_1 \times M_2 \times K}$, given by

$$\boldsymbol{\mathcal{H}} = \sum_{l=1}^{L} \breve{\alpha}_l \, \boldsymbol{a}_{l,1}^{(M_1)} \circ \boldsymbol{a}_{l,2}^{(M_2)} \circ \boldsymbol{a}_{l,3}^{(k)} \bullet \boldsymbol{\mathcal{D}}_l, \tag{4}$$

where $\boldsymbol{a}_{l,1}^{(M_1)}$, $\boldsymbol{a}_{l,2}^{(M_2)}$, and $\boldsymbol{a}_{l,3}^{(K)}$ are steering vectors formed by $\exp(-j2\pi m_1 \phi_{l,1})$, $\exp(-j2\pi m_2 \phi_{l,2})$, and $\exp(-j2\pi k \Delta f \tau_l)$. The phase rotation tensor $\boldsymbol{\mathcal{D}}_l \in \mathbb{C}^{M_1 \times M_2 \times K}$ is produced by the wideband effect, with entries $d_{l,m_1,m_2,k} = \exp(-j2\pi k \Delta f (m_1 \phi_{l,1}/f_\mathrm{c} + m_2 \phi_{l,2}/f_\mathrm{c}))$.

Remark 1 (Narrowband model)**.** *The narrowband model relies on the approximation $\phi_{l,k,i} = \phi_{l,i}$, $\forall k$, or, equivalently, $\boldsymbol{\mathcal{D}}_l \equiv \mathbf{1} \in \mathbb{C}_1^M \times M_2 \times K$. The narrowband channel model is of the standard form for MD-ESPRIT [18] and other tensor-based methods, therefore, such methods can be directly applied.*

Proposition 1 (Revised narrowband condition)**.** *The narrowband model holds when $d_{l,m_1,m_2,k} \approx 1$, which is fulfilled when $2\pi(M_1 + M_2)K\Delta f d_i/(f_c \lambda_c) \ll 1$.*

Proof. In order to investigate the condition when the wideband channel converges to the narrowband channel, we employ the perturbation analysis as a tool [22]. Consider any path l, the entries in $\boldsymbol{\mathcal{D}}_l$ are given by $d_{l,m_1,m_2,k} = \exp(\psi_{l,m_1,m_2,k})$, for some $\psi_{l,m_1,m_2,k} \in \mathbb{C}$. The wideband effect causes a perturbation $\Delta\psi_{l,m_1,m_2,k}$ from 0. From the perspective of channel, it eventually causes $\Delta d_{l,m_1,m_2,k}$ in the tensor $\boldsymbol{\mathcal{D}}_l$, which differs from the narrowband channel. The value of $\Delta d_{l,m_1,m_2,k}$ as a result of perturbation $\Delta\psi_{l,m_1,m_2,k}$ is given

[3] If L is unknown, the model order estimation algorithm based on (4) can be performed, as indicated in [9].

by Taylor expansion at $\psi_{l,m_1,m_2,k} = 0$, which yields (dropping all indices)

$$\Delta d = e^{\psi} - e^{0} \approx \left.\frac{\mathrm{d}e^{\psi}}{\mathrm{d}\psi}\right|_{\psi=0} (\psi - 0) = \psi. \tag{5}$$

Hence, the perturbation caused by input $\Delta\psi_{l,m_1,m_2,k}$ leads to an identical output perturbation, i.e., $\Delta d_{l,m_1,m_2,k} = \Delta\psi_{l,m_1,m_2,k}$. For the narrowband condition to hold, we require

$$\max_{l,m_1,m_2,k} |\Delta d_{l,m_1,m_2,k}| \ll e^{0}. \tag{6}$$

The maximal possible values are jointly given by $m_1 = M_1 - 1$, $m_2 = M_2 - 1$, $k = K - 1$, and $\phi_{l,i} = d_i/\lambda_{\mathrm{c}}$, which, combined with the expression of $d_{l,m_1,m_2,k}$ in Section III-A, leads to the specified condition. □

The revised narrowband condition will be confirmed numerically in Section IV. For $d_i = \lambda_{\mathrm{c}}/2$, the condition can be further simplified to $\pi(M_1 + M_2)B \ll f_{\mathrm{c}}$.

Remark 2 (On auto-pairing)**.** *When $\boldsymbol{\mathcal{D}}_l = \mathbf{1}$, $\forall l$, a unique tensor decomposition with simultaneous diagonalization operation ensures auto-pairing. However, when $\boldsymbol{\mathcal{D}}_l \neq \mathbf{1}$, the non-singular matrix used for diagonalization is not the same over different subcarriers, hence auto-pairing across subcarriers is no longer guaranteed.*

B. Proposed Method

The proposed channel estimation method comprises three phases: 1) per subcarrier processing, 2) across subcarrier pairing, and 3) delay and complex gain estimation. While a detailed complexity analysis is beyond the scope of the paper, we note that the complexity of the proposed method has the same scaling as [19].

1) Phase 1: Parallel MD-ESPRIT: Extracting the channel response over the k-th subcarrier, we form the channel matrix $\hat{\boldsymbol{H}}_k$, which can be written as

$$\hat{\boldsymbol{H}}_k = \sum_{l=1}^{L} \hat{\gamma}_{l,k} \hat{\boldsymbol{a}}_{l,k,1}^{(M_1)} \hat{\boldsymbol{a}}_{l,k,2}^{(M_2)\top}, \tag{7}$$

where $\hat{\gamma}_{l,k} = \hat{\alpha}_l \exp(-j2\pi(f_{\mathrm{c}} + k\Delta f)\hat{\tau}_l)$, and $\hat{\boldsymbol{a}}_{l,k,i}^{(M_i)}$ is steering vector formed by i-th mode of l-th path, i.e., $\hat{a}_{l,k,i} = \exp(-j2\pi(1 + k\Delta f/f_{\mathrm{c}})\hat{\phi}_{l,i})$. By applying the MD-ESPRIT algorithm from [18] to (7) for each k, the outputs are the paired modes $(\hat{a}_{l,k,1}, \hat{a}_{l,k,2})$. The paired angles $(\hat{\phi}_{l,1}^{[k]}, \hat{\phi}_{l,2}^{[k]})$ associated with each subcarrier are then calculated as

$$\hat{\phi}_{l,i}^{[k]} = -\frac{f_{\mathrm{c}}}{2\pi(f_{\mathrm{c}} + k\Delta f)} \Im(\ln(\hat{a}_{l,k,i})). \tag{8}$$

Although the AOA and AOD are auto-paired on each subcarrier, the ordering is not maintained across subcarriers, i.e., $(\hat{\phi}_{l,1}^{[k]}, \hat{\phi}_{l,2}^{[k]})$ and $(\hat{\phi}_{l,1}^{[k']}, \hat{\phi}_{l,2}^{[k]})$ do not necessarily pertain to the same path l, for $k \neq k'$. This is because the singular values output of SVD within MD-ESPRIT are in descending order, i.e., ordered based on the received signal strength of the paths. Due to the noise and frequency selective fading effects, the order of signal strength of paths varies across subcarriers. For this reason, all methods involving SVD techniques in a parallel architecture, such as [19] or tensor-based method including per subcarrier processing, will encounter the pairing problem across subcarriers.

2) Phase 2: Pairing Across Subcarriers: Increasing SNR can alleviate the pairing problem. However, there are often limitations on transmission energy and hardware. The traditional pairing method that utilizes the same eigenstructure can not be applied here since the eigenstructure per subcarrier differs. Our approach based on a modified K-means algorithm [23, Ch. 9] avoids the need for high SNR. We introduce KL vectors $\mathbf{y}_{(l-1)k+k} = [\hat{\phi}_{l,1}^{[k]}, \hat{\phi}_{l,2}^{[k]}]^\top$. We now index these measurements as $\mathbf{y}_n$, $n = 1, \ldots, N$, where $N = KL$. The initialization of K-means is random, with $\boldsymbol{\mu}_j \in [-\pi/2, \pi/2] \times [-\pi/2, \pi/2]$, $j = 1, \ldots, L$. The assignments $r_{n,j} \in \{0, 1\}$ and the means $\boldsymbol{\mu}_j$ are updated iteratively as

$$r_{n,j} = \begin{cases} 1 & j = \mathrm{argmin}_{j'} D(\mathbf{y}_n, \boldsymbol{\mu}_{j'}) \\ 0 & \text{otherwise}, \end{cases} \tag{9}$$

and

$$\boldsymbol{\mu}_j = \frac{\sum_{n=1}^{N} r_{n,j}\mathbf{y}_n}{\sum_{n=1}^{N} r_{n,k}}, \tag{10}$$

where $D(\cdot,\cdot)$ is a suitable distance metric that accounts for any angle wrapping. In our case, we have set $D(\mathbf{y}_n, \boldsymbol{\mu}_{j'}) = \|\mathbf{y}_n - \boldsymbol{\mu}_{j'}\|$, as we operate in an SNR regime where angle wrapping is rare. We repeat (9)–(10) until there is no further change in the assignments, i.e., $r_{n,j}$ remains unchanged. Since the K-means algorithm is ignorant of the constraint that $\mathbf{y}_{(l-1)k+k}$ and $\mathbf{y}_{(l'-1)k+k}$ are not allowed to be in the same cluster for $l' \neq l$, we check for each cluster if more than one measurement with the same subcarrier index is present. If so, we only retain the one closest to the cluster means and discard the others. Then the cluster means are recomputed. Finally, $\hat{\phi}_{l,1}$ and $\hat{\phi}_{l,2}$ are obtained from the means $[\hat{\phi}_{l,1}, \hat{\phi}_{l,2}]^\top = \boldsymbol{\mu}_l$. Once $\hat{\phi}_{l,i}$ is obtained, physical AOD and AOA are calculated by $\hat{\theta}_{l,i} = \arcsin(\hat{\phi}_{l,i}\lambda_{\mathrm{c}}/d_i)$.

3) Phase 3: Delay and Complex Gain Estimation: It can be verified that the channel matrix over the k-th subcarrier admitted the following form of matrix product

$$\hat{\boldsymbol{H}}_k = \hat{\boldsymbol{A}}_{k,1}^{(M_1)} \mathrm{diag}(\hat{\boldsymbol{\gamma}}_k) \hat{\boldsymbol{A}}_{k,2}^{(M_2)\top}, \tag{11}$$

where $\hat{\boldsymbol{\gamma}}_k$ is a vector formed by $\hat{\gamma}_{l,k}$ and $\hat{\boldsymbol{A}}_{k,i}^{(M_i)} = [\hat{\boldsymbol{a}}_{1,k,i}^{(M_i)} \cdots \hat{\boldsymbol{a}}_{l,k,i}^{(M_i)} \cdots \hat{\boldsymbol{a}}_{L,k,i}^{(M_i)}]$. The mode of $\hat{\boldsymbol{a}}_{1,k,i}^{(M_i)}$ can be reconstructed from the estimates of $\hat{\phi}_{l,i}$ after pairing as described in Sec.III-B1. Then $\hat{\boldsymbol{\gamma}}_k$ can be calculated as

$$\hat{\boldsymbol{\gamma}}_k = (\hat{\boldsymbol{A}}_{k,1}^{(M_1)} \odot \hat{\boldsymbol{A}}_{k,2}^{(M_2)})^\dagger \mathrm{vec}_{\mathrm{r}}(\hat{\boldsymbol{H}}_k), \tag{12}$$

so that $\hat{\gamma}_{l,k}$ can be obtained for all subcarriers. Take the complex logarithm of $\hat{\gamma}_{l,k} = \hat{\alpha}_l e^{-j2\pi(f_{\mathrm{c}}+k\Delta f)\hat{\tau}_l}$ and stacking the values into vector $\hat{\boldsymbol{\gamma}}_l$, we find that

$$\ln(\hat{\boldsymbol{\gamma}}_l) = \ln(\hat{\alpha}_l)\mathbf{1} + \hat{\tau}_l \boldsymbol{s}, \tag{13}$$

where $s_k = -j2\pi(f_{\mathrm{c}} + k\Delta f)$. Introducing $\boldsymbol{S} = [\boldsymbol{s}\,\mathbf{1}]$, then the least squares (LS) estimate of delay and channel gain are

$$\begin{bmatrix} \hat{\tau}_l \\ \ln(\hat{\alpha}_l) \end{bmatrix} = \boldsymbol{S}^\dagger \ln(\hat{\boldsymbol{\gamma}}_l). \tag{14}$$

For the noisy channel, we can take $\Re\{\hat{\tau}_l\}$ as the estimated delay (containing clock bias).

C. Localization

For the LOS path, the UE location is expressed as:

$$\boldsymbol{p}_2 = \boldsymbol{p}_1 + c(\hat{\tau}_1 - \Delta\tau)\hat{\boldsymbol{f}}_{1,2}, \tag{15}$$

where both $\boldsymbol{p}_2$ and $\Delta\tau$ are unknown. For the NLOS paths, the UE position can be expressed in $\hat{\theta}_{l,1}$, $\hat{\theta}_{l,2}$ and $\hat{\tau}_l$ of each path according to geometry as (16) [24].

$$\boldsymbol{p}_2 = \boldsymbol{p}_1 + \hat{\boldsymbol{f}}_{l,1} d_l + (c(\hat{\tau}_l - \Delta\tau) - d_l)\hat{\boldsymbol{f}}_{l,2}, \tag{16}$$

where $\boldsymbol{p}_2$ and $\boldsymbol{p}_1$ denote the UE's position and BS's position, respectively, $\hat{\boldsymbol{f}}_{l,1}$ and $\hat{\boldsymbol{f}}_{l,2}$ represent directional vectors corresponding to the departure and arrival of the signal, respectively, given by $\hat{\boldsymbol{f}}_{l,2} = [\cos(\hat{\theta}_{l,2}), -\sin(\hat{\theta}_{l,2})]^\top$, $\hat{\boldsymbol{f}}_{l,1} = [\cos(\hat{\theta}_{l,1}), \sin(\hat{\theta}_{l,1})]^\top$, and $d_l = \|\boldsymbol{p}_1 - \boldsymbol{p}_l'\|$ represents the unknown travel distance of electromagnetic waves before reflection. Let $\hat{\boldsymbol{f}}_l = -(\hat{\boldsymbol{f}}_{l,2} + \hat{\boldsymbol{f}}_{l,1})$, joint equations given by (15) and (16) can be written as $\boldsymbol{B}\boldsymbol{v} = \boldsymbol{z}$, where

$$\boldsymbol{B} = \begin{bmatrix} \boldsymbol{I}_{2\times2} & c\hat{\boldsymbol{f}}_{1,2} & \boldsymbol{0}_{2\times1} & \boldsymbol{0}_{2\times1} & \cdots & \boldsymbol{0}_{2\times1} \\ \boldsymbol{I}_{2\times2} & c\hat{\boldsymbol{f}}_{2,2} & \hat{\boldsymbol{f}}_2 & \boldsymbol{0}_{2\times1} & \cdots & \boldsymbol{0}_{2\times1} \\ \boldsymbol{I}_{2\times2} & c\hat{\boldsymbol{f}}_{3,2} & \boldsymbol{0}_{2\times1} & \ddots & \ddots & \vdots \\ \vdots & \vdots & \vdots & \ddots & \ddots & \boldsymbol{0}_{2\times1} \\ \boldsymbol{I}_{2\times2} & c\hat{\boldsymbol{f}}_{L,2} & \boldsymbol{0}_{2\times1} & \cdots & \boldsymbol{0}_{2\times1} & \hat{\boldsymbol{f}}_L \end{bmatrix} \tag{17}$$

and $\boldsymbol{v} = [\boldsymbol{p}_2^\top, \Delta\tau, d_2, \cdots, d_L]^\top$, $\boldsymbol{z} = [\boldsymbol{p}_1^\top + c\hat{\tau}_l\hat{\boldsymbol{f}}_{1,2}^\top, \cdots, \boldsymbol{p}_1^\top + c\hat{\tau}_L\hat{\boldsymbol{f}}_{L,2}^\top]^\top$. The least square method gives that $\boldsymbol{v} = \boldsymbol{B}^\dagger\boldsymbol{z}$, the estimates $\boldsymbol{p}_2$ and $\Delta\tau$ are obtained by extracting the first three entries in $\boldsymbol{v}$. Measurements from total L paths can establish $2L$ equations containing $L+2$ unknowns. The equations are over-determined and can be solved when $L \geq 2$.

IV. Simulation

A. System Setup

The MIMO-OFDM localization scenario is set up as follows: The BS is equipped with $M_1 = 32$ ULA antennas at $(0, 40)$m, whereas the UE is equipped with $M_2 = 32$ ULA antennas at $(40, 0)$m. The antenna spacing at both sides equals to half wavelength. The BS sends symbols with total transmitted power $P_\mathrm{t} = 15$ dBm and synchronization error is assumed to be $\Delta\tau = 0.5\,\mathrm{ms}$. The system bandwidth is $B = K\Delta f$ with subcarrier spacing $\Delta f = 120\,\mathrm{kHz}$, and the carrier frequency is $f_\mathrm{c} = 28\,\mathrm{GHz}$. For these parameter settings,[4] the narrowband thresholds are 87.5 MHz [15] and 13.9 MHz (from Proposition 1), where in both cases '$\ll$' is interpreted as '10 times smaller'. The number of pilots for obtaining the estimate (3) is $n_\mathrm{p} = 64$. The (AOD, AOA) of paths are set as $(-45°, 45°)$, $(-54°, -62°)$, $(65°, 40°)$. The noise power spectral density (PSD) is $N_0 = -174\,\mathrm{dBm}$ and the noise figure (NF) $n_f = 8\mathrm{dB}$. The energy loss of reflection is set to $3\,\mathrm{dB}$.

We evaluate three methods in terms of the root-mean-square error (RMSE) of the channel parameter and the position estimation: (i) the proposed method. (ii) the method from [19]

[4]The RMSE results as a function of the carrier frequency f_c with fixed B show that the performance of the different methods converges as f_c increases. Results are omitted for space reasons.

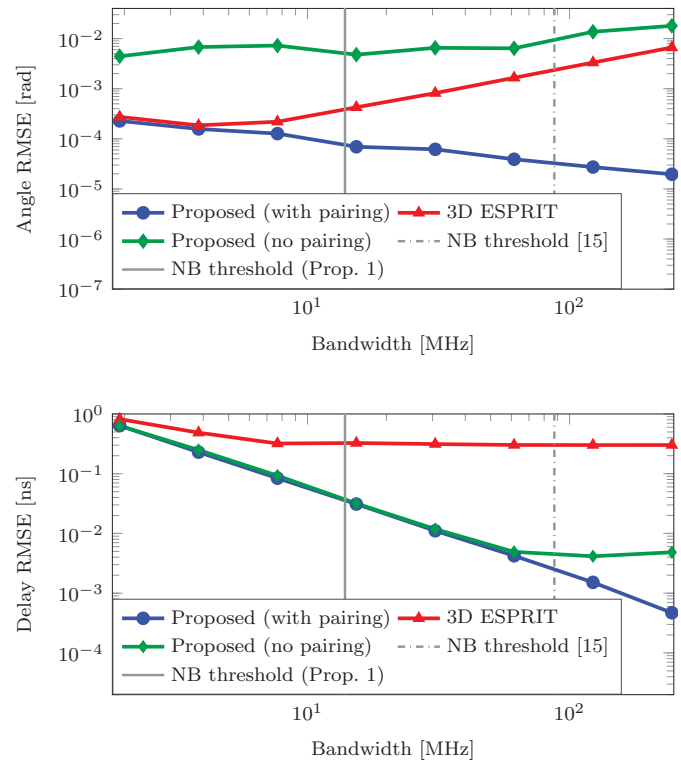

Fig. 2: Channel parameter RMSE as a function of the bandwidth, for AOA estimation (top) and delay estimation (bottom), along with the narrowband (NB) conditions from [15] and Proposition 1.

without pairing, but replacing IMDF with MD-ESPRIT.[5] For angle estimation, we implement the proposed method without the pairing step. For delay estimation described in Section III-B3, we use $\hat{\phi}_{l,k,i}$ to reconstruct $\hat{\boldsymbol{A}}_{k,i}^{(M_i)}$; (iii) standard 3D ESPRIT, which ignores the wideband effect [18] and directly compute angles and delays; For all methods, the localization is performed as Section III-C.

B. Results and Discussion

1) Channel Parameter Estimation: In Fig. 2, we show the AOA[6] and delay estimation as a function of the bandwidth. We observe that AOA estimation RMSE from 3D ESPRIT first increased with larger bandwidth, due to the increasing samples and tolerable wideband effect. With larger bandwidth, however, the wideband effect becomes dominant compared to noise, and the AOA RMSE quickly increases. The angle RMSE of the proposed method always decreases with a larger bandwidth. ´ In terms of delay RMSE, the 3D ESPRIT method exhibits near-constant performance. This is because 3D ESPRIT does average in each dimension, and the dimension containing delay information is not affected by the wideband effect. For the proposed method, the delay RMSE keeps decreasing due to improving accuracy of $\hat{\boldsymbol{A}}_{k,i}^{(M_i)}$ reconstruction in (11) as a result of improved angle estimation. The delay

[5]We recall that MD-ESPRIT has been shown to outperform IMDF in [19] and the MD-ESPRIT does not require multiple snapshot observations. Hence, by removing the weaknesses of IMDF, a more fair comparison is conducted, with focus on the pairing issue.

[6]AOD performance is not shown as it is similar to AOA performance.

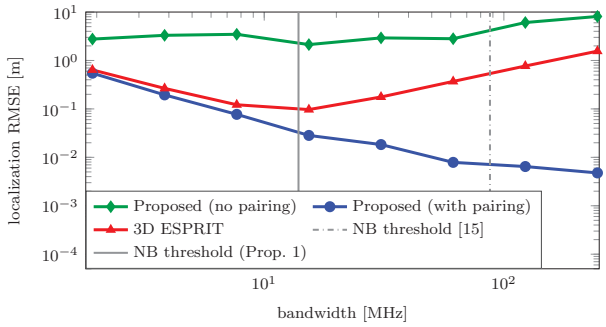

Fig. 3: Localization RMSE as a function of the bandwidth for the proposed method (with and without pairing), compared to the standard 3D ESPRIT with auto-pairing, along with the narrowband (NB) conditions from [15] and Proposition 1.

estimation without pairing first improves due to increasing SNR, then remains stable, as it is limited by reconstruction accuracy of $\hat{\boldsymbol{A}}_{k,i}^{(M_i)}$, since the angle estimation per subcarrier are of the same accuracy and there is no way to harness SNR gain by fusing across the subcarriers.

2) Localization: From Fig. 3, the localization RMSE of the proposed method monotonically improves when larger bandwidth is applied as a consequence of continuously improving the accuracy of angle and delay estimation. The localization RMSE of wideband 3D ESPRIT initially goes down due to improvement of delay estimation, however, it starts to diverge after about 15MHz due to poor angle RMSE. The localization without proper pairing causes large errors, due to the poor AOA and AOD estimates. From Figs. 2–3, we see that the wideband effect has taken place prior to the threshold in [15]. The importance of correct pairing across subcarriers is evident, as improper pairing causes a significant error as shown in Figs. 2–3.

V. Conclusions

In this paper, we proposed a new method to deal with the spatial wideband effect with one snapshot observation. As part of this method, we investigate the pairing problem that will universally appear in methods that involve SVD or HOSVD and per-subcarrier processing, and propose a strategy to address this problem. Furthermore, we provided a tighter narrowband condition. Finally, we demonstrate that the wideband effect significantly degrades localization performance, if not properly addressed.

References

[1] M. A. Uusitalo, P. Rugeland, M. R. Boldi, and et al, "6G vision, value, use cases and technologies from european 6G flagship project Hexa-X," *IEEE Access*, vol. 9, pp. 160 004–160 020, 2021.

[2] N. Gupta, S. Sharma, P. K. Juneja, and U. Garg, "SDNFV 5G-IoT: A framework for the next generation 5G enabled IoT," in *IEEE Conference on Advances in Computing, Communication & Materials (ICACCM)*, 2020, pp. 289–294.

[3] H. Chen, H. Sarieddeen, T. Ballal, H. Wymeersch, M.-S. Alouini, and T. Y. Al-Naffouri, "A tutorial on terahertz-band localization for 6G communication systems," *IEEE Communications Surveys & Tutorials*, 2022.

[4] R. Karlsson and F. Gustafsson, "The future of automotive localization algorithms: available, reliable, and scalable localization: anywhere and anytime," *IEEE signal processing magazine*, vol. 34, no. 2, pp. 60–69, 2017.

[5] F. Jiang, F. Wen, Y. Ge, M. Zhu, H. Wymeersch, and F. Tufvesson, "Beamspace multidimensional ESPRIT approaches for simultaneous localization and communications," *arXiv:2111.07450v1*, 2021.

[6] F. Wen, J. Kulmer, K. Witrisal, and H. Wymeersch, "5G positioning and mapping with diffuse multipath," *IEEE Transactions on Wireless Communications*, vol. 20, no. 2, pp. 1164–1174, 2021.

[7] F. Jiang, Y. Ge, M. Zhu, and H. Wymeersch, "High-dimensional channel estimation for simultaneous localization and communications," in *IEEE WCNC*, Nanjing, China, 2021.

[8] J. Zhang and M. Haardt, "Channel estimation and training design for hybrid multi-carrier mmwave massive MIMO systems: The beamspace ESPRIT approach," in *IEEE EUSIPCO*, Kos, 2017.

[9] Y. Ge, F. Wen, H. Kim, M. Zhu, F. Jiang, S. Kim, L. Svensson, and H. Wymeersch, "5G SLAM using the clustering and assignment approach with diffuse multipath," *Sensors*, vol. 20, no. 16, p. 4656, Aug. 2020.

[10] R. W. Heath, N. González-Prelcic, S. Rangan, W. Roh, and A. M. Sayeed, "An overview of signal processing techniques for millimeter wave MIMO systems," *IEEE Journal of Selected Topics in Signal Processing*, vol. 10, no. 3, pp. 436–453, 2016.

[11] J. Lee, G.-T. Gil, and Y. H. Lee, "Channel estimation via orthogonal matching pursuit for hybrid MIMO systems in millimeter wave communications," *IEEE Transactions on Communications*, vol. 64, no. 6, pp. 2370–2386, 2016.

[12] Y. Tsai, L. Zheng, and X. Wang, "Millimeter-wave beamformed full-dimensional MIMO channel estimation based on atomic norm minimization," *IEEE Transactions on Communications*, vol. 66, no. 12, pp. 6150–6163, 2018.

[13] A. Liao, Z. Gao, H. Wang, S. Chen, M.-S. Alouini, and H. Yin, "Closed-loop sparse channel estimation for wideband millimeter-wave full-dimensional mimo systems," *IEEE Transactions on Communications*, vol. 67, no. 12, pp. 8329–8345, 2019.

[14] B. Wang, M. Jian, F. Gao, G. Y. Li, and H. Lin, "Beam squint and channel estimation for wideband mmwave massive MIMO-OFDM systems," *IEEE Transactions on Signal Processing*, vol. 67, no. 23, pp. 5893–5908, 2019.

[15] B. Wang, F. Gao, S. Jin, H. Lin, and G. Y. Li, "Spatial-and frequency-wideband effects in millimeter-wave massive MIMO systems," *IEEE Transactions on Signal Processing*, vol. 66, no. 13, pp. 3393–3406, 2018.

[16] M. Sørensen and L. Lathauwer, "Multidimensional harmonic retrieval via coupled canonical polyadic decomposition—Part I: model and identifiability," *IEEE Transactions on Signal Processing*, vol. 65, no. 2, pp. 517–527, Jan. 2016.

[17] J. Liu, X. Liu, and X. Ma, "Multidimensional frequency estimation with finite snapshots in the presence of identical frequencies," *IEEE Transactions on Signal Processing*, vol. 55, no. 11, pp. 5179–5194, Nov. 2007.

[18] S. Sahnoun, K. Usevich, and P. Comon, "Multidimensional ESPRIT for damped and undamped signals: algorithm, computations, and perturbation analysis," *IEEE Transactions on Signal Processing*, vol. 65, no. 22, pp. 5897–5910, Nov. 2017.

[19] Y. Lin, S. Jin, M. Matthaiou, and X. You, "Tensor-based channel estimation for millimeter wave MIMO-OFDM With dual-wideband effects," *IEEE Transactions on Communications*, vol. 68, no. 7, pp. 4218–4232, 2020.

[20] M. Haardt, F. Roemer, and G. Del Galdo, "Higher-order SVD-based subspace estimation to improve the parameter estimation accuracy in multidimensional harmonic retrieval problems," *IEEE Transactions on Signal Processing*, vol. 56, no. 7, pp. 3198–3213, 2008.

[21] F. Jiang, C. Li, and Z. Gong, "Accurate analytical BER performance for ZF receivers under imperfect channel in low-SNR region for large receiving antennas," *IEEE Signal Process. Lett.*, vol. 25, no. 8, pp. 1246–1250, Aug. 2018.

[22] Z. Xu, "Perturbation analysis for subspace decomposition with applications in subspace-based algorithms," *IEEE Transactions on Signal Processing*, vol. 50, no. 11, pp. 2820–2830, 2002.

[23] C. M. Bishop and N. M. Nasrabadi, *Pattern recognition and machine learning*. Springer, 2006, vol. 4, no. 4.

[24] F. Wen and H. Wymeersch, "5G synchronization, positioning, and mapping from diffuse multipath," *IEEE Wireless Communications Letters*, vol. 10, no. 1, pp. 43–47, 2021.